Published in final edited form as:
Cancer Res. 2013 January 15; 73(2): 529–538. doi:10.1158/0008-5472.CAN-12-3461.

Hyperpolarized ^{13}C-pyruvate magnetic resonance reveals rapid lactate export in metastatic renal cell carcinomas

Kayvan R. Keshari[1,a], **Renuka Sriram**[1], **Bertram L. Koelsch**[2], **Mark Van Criekinge**[1], **David M. Wilson**[1], **John Kurhanewicz**[1,2], and **Zhen J. Wang**[1]

[1]Department of Radiology and Biomedical Imaging, University of California, San Francisco, San Francisco, CA 94143, USA

[2]UC Berkeley – UCSF Graduate Program in Bioengineering, San Francisco, CA 94143, USA

Abstract

Renal cell carcinomas (RCCs) are a heterogeneous group of tumors with a wide range of aggressiveness. Noninvasive methods to confidently predict the tumor biological behavior and select appropriate treatment are lacking. Here, we investigate the dynamic metabolic flux in living RCC cells using hyperpolarized ^{13}C-pyruvate magnetic resonance spectroscopy (MRS) combined with a bioreactor platform, and interrogated the biochemical basis of the MRS data with respect to cancer aggressiveness. RCC cells have significantly higher pyruvate-to-lactate flux than the normal renal tubule cells. Furthermore, a key feature distinguishing the localized from the metastatic RCC cells is the lactate efflux rate, mediated by the monocarboxylate transporter 4 (MCT4). The metastatic RCC cells have significantly higher MCT4 expression and corresponding higher lactate efflux, which is essential for maintaining a high rate of glycolysis. We show that such differential cellular transporter expression and associated metabolic phenotype can be noninvasively assessed via real-time monitoring of hyperpolarized ^{13}C-pyruvate-to-lactate flux.

Keywords

metabolic flux; monocarboxylate transporter; lactate efflux; bioreactor; magnetic resonance spectroscopy

Introduction

The incidence of renal tumors, both malignant renal cell carcinomas (RCCs) and benign renal tumors, has risen significantly in the last 20 years (1). In the case of renal tumors, biopsies are not routinely done, due to the risk of hemorrhage and high likelihood of indeterminate histology (2, 3). Treatment selection is thus heavily reliant on non-invasive imaging assessment of tumor masses. However, there are significant limitations to the current imaging methods for renal tumor characterization. It is increasingly recognized that RCCs are a heterogeneous group of tumors with a wide range of biological aggressiveness (4, 5). Emerging active surveillance data have shown that a significant percentage of small RCCs (< 4cm) are indolent with low metastatic risk, and patients may be over-treated if all such RCCs are surgically removed (5, 6). On the other hand, 20–40% of patients undergoing nephrectomies for clinically localized RCCs develop metastases with poor outcome (7).

[a]Correspondence and Reprint request: Kayvan R. Keshari, Ph.D. Department of Radiology and Biomedical Imaging, University of California, San Francisco, 1700 4th St. Byers Hall 203 San Francisco, CA 94158, Phone: (415) 514-9717, Fax: (415) 514-9711, kayvan.keshari@ucsf.edu.

No Conflict of Interest

Unfortunately, current imaging methods cannot reliably predict the risks of progression from localized RCC to metastatic disease (8). Furthermore, certain benign renal tumors are difficult to distinguish from RCCs by imaging (9). This diagnostic challenge has resulted in the unnecessary resection of many benign renal tumors, which constitute 20% of all renal tumors <4cm, with the associated surgical risks and potential loss of renal function (10). Therefore, new imaging methods are needed to predict the biological behavior of renal tumors and select appropriate treatment.

The unique metabolism of cancer cells is central to their malignant behavior. For example, a common property of cancers is altered glucose metabolism with elevated glycolysis and lactate production in the presence of oxygen (11, 12). Increased glycolysis facilitates the uptake and incorporation of nutrients and biomass needed for cell proliferation in cancers (13, 14), and acidifies the extracellular microenvironment promoting invasion of neighboring tissue and metastasis (15). A number of genomics and proteomics studies have demonstrated increased metabolism to lactate in RCCs (16–19). Specifically, proteomic analysis of RCC tissues and metabolic profiling of serum samples revealed increased levels of glycolytic enzymes in RCC tissues and higher lactate in the serum of RCC patients (19). Metastatic RCCs have also demonstrated a bio-energetic shift toward aerobic glycolysis and lactate production (18). These studies provide the rationale for metabolic imaging of glycolysis as a non-invasive means to characterize renal tumor aggressiveness.

Hyperpolarized (HP) ^{13}C MR is a new molecular imaging technique that allows rapid and noninvasive monitoring of dynamic pathway-specific metabolic and physiological processes. Hyperpolarization, achieved through the dynamic nuclear polarization (DNP) technique (20), can provide dramatic gains in sensitivity (> 10,000-fold increase) for imaging ^{13}C-labeled bio-molecules. The HP ^{13}C-probes can be injected into living systems, and their metabolism can be observed in real-time by chemical shift. The most commonly used HP ^{13}C probe is ^{13}C-pyruvate, which is at the juncture of several important energy and biosynthetic pathways. For example, pyruvate may be converted to lactate in glycolysis, to acetyl-CoA to support the tricarboxylic acid (TCA) cycle, or to alanine via transamination for protein synthesis. HP ^{13}C-pyruvate MR has already been applied to the detection of the presence (21–25) and progression (26, 27) of a number of cancers. The metabolic changes seen in RCCs suggest that HP ^{13}C-pyruvate will also be an excellent probe to interrogate these tumors noninvasively.

In this work, we compared the pyruvate metabolism of immortalized cells derived from human renal proximal tubules (the origin of most human RCCs), a localized human RCC, and a metastatic human RCC, with the goal of identifying clinically translatable HP biomarkers of renal tumor aggressiveness. After evaluating the steady-state metabolism of these cells, we assessed the dynamic HP pyruvate-to-lactate flux using a MR compatible bioreactor platform that provides a controlled and physiological setting for the cells (28). By monitoring the real time metabolic flux using HP MR, we showed that RCC cells have significantly higher pyruvate-to-lactate flux than the normal renal proximal tubule cells. Furthermore, we showed that cells derived from the metastatic RCC have more rapid export of lactate to the extracellular space compared to the cells derived from the localized RCC, and that these differences are likely mediated by the differential expression of monocarboxylate transporter 4 (MCT4). These results suggest that using HP ^{13}C-pyruvate to assess lactate production and export has the potential to improve the non-invasive characterization of renal tumors.

Materials and Methods

Cell lines

HK-2 is an immortalized proximal tubule epithelial cell line from normal adult human kidney (29), and was obtained from American Type Culture Collection (ATCC, Virginia; obtained June, 2010; authentication performed at ATCC was via Short Tandem Repeat (STR) Profiling). UMRC6 cells are representative of localized human clear cell renal cell carcinoma (30), and were a gift from Dr. Bart Grossman (MD Anderson Cancer Center; obtained January, 2010; authenticated using STR Profiling, October 2012). UOK262 cells are derived from a metastasis of the highly aggressive hereditary leiomyomatosis renal cell carcinoma (HLRCC), which is characterized by mutation of the TCA cycle enzyme fumarate hydratase (FH) (31). UOK262 cells were a gift from Dr. W. Marston Linehan (National Cancer Institute; obtained May, 2010; authenticated using STR Profiling, October 2012). All cells were grown in Dulbeco's Modified Eagle's medium (DMEM) with 4.5g/L glucose. The cells were passaged serially and were used for assays and MR experiments between passages 2–10 and at 60–80% confluency.

^{1}H NMR experiments

Cells were plated on 150-cm^2 coated petri dishes (Fisher Scientific) and incubated for 24-hours in DMEM media supplemented with [1-^{13}C] glucose, or for 2-hours in DMEM media supplemented with [3-^{13}C] pyruvate (Cambridge Isotope Labs, MA). At the end of incubation, an aliquot of medium was collected, and cells were extracted in ice-cold methanol (32). The cell extracts were reconstituted in D_2O with known amounts of trimethyl silyl pentanoate (TSP) for internal reference. The extracts were measured on Bruker Advance III 800MHz equipped with a cryo-cooled triple resonance probe. High-resolution water-suppressed proton spectra were obtained with a repetition time of 12s and 64 averages. The metabolite peak areas were quantified against the known TSP peak area.

Hyperpolarized [1-^{13}C] pyruvate MR Bioreactor experiment

Cells were electrostatically encapsulated into 2.5% weight/volume alginate microspheres as previously described (28, 33), and then loaded into a MR-compatible bioreactor. Approximately 800μL of microspheres were perfused in the bioreactor with DMEM H-21 media at a flow rate of 2.5mL/min. For the flow rate modulation bioreactor experiments, the flow rate was changed to either 1.3mL/min or 3.8mL/min for the duration of the hyperpolarized scans. The media was kept at 37°C with water-jacketed perfusion lines and was maintained at 95% air/5% CO_2 via gas exchanger. All bioreactor studies were performed on a 500MHz Varian Inova (Agilent Technologies, CA) with a 10mm, triple-tune, direct-detect, broadband probe at 37°C. For the hyperpolarized ^{13}C-pyruvate studies, 2.5uL of 14.2M ^{13}C-pyruvate mixed with 15mM of the trityl radical (GE Healthcare) was polarized on a Hypersense polarizer (Oxford Instruments, UK). This was followed by dissolution in 5mL of 50mM phosphate buffer. 1 mL of the resulting 7.5mM HP pyruvate solution was injected into the bioreactor containing the microspheres. Hyperpolarized ^{13}C MR data were acquired dynamically with a 10° flip-angle, pulse repetition time of 3s and for a duration of 300s. ^{31}P spectra (repetition time 3s, 1024 averages, 90° flip-angle) were acquired before and after each hyperpolarized study to assess cell viability.

Cell number determination for bioreactor experiments

Moles of ATP per cell for each cell line were measured using CellTiter-Glo luminescent cell viability assay and Veritas Luminometer (Promega, WI). Moles of ATP corresponding to the β-NTP peak area on ^{31}P spectra were determined using a ^{31}P calibration curve. The number of cells in each bioreactor experiment was then calculated by dividing the moles of

ATP approximated from β-NTP peak by the moles of ATP per cell as measured by the luminescent assay.

mRNA expression and enzyme activity assay

Total RNA was purified from cells using RNeasy procedure kit (Qiagen, USA), and reverse transcribed using iScript cDNA Synthesis kit (BioRad Laboratories, CA). PCR was conducted in triplicate for the lactate dehydrogenase α(LDH-α) and the monocarboxylate transporters 1 and 4 (Hs00161826_m1, Hs00358829_m1) on the ABI 7900HT (Applied Biosystems, CA). Cyclophilin and beta Actin (Applied Biosystems, CA) were used as control, and the relative fold difference was calculated for each primer/probe combination.

LDH activity of cell lysates was measured spectrophotometrically by quantifying the linear decrease in nicotinamide adenine dinucleotide (NADH) absorbance at varying pyruvate concentrations at 339 nm using a microplate reader (Tecan Group Ltd., Switzerland). The maximum velocity (Vmax) and the Michaelis-Menten constant (Km) were estimated using the Lineweaver-Burke plot.

Data analysis

The hyperpolarized pyruvate-to-lactate flux was calculated using a previously published model (28). The pyruvate-to-lactate flux was normalized by the number of cells in each bioreactor study and the injected amount of hyperpolarized pyruvate. ^{31}P metabolite peaks were integrated and normalized by the number of cells to determine the concentration of phosphocholine (PC), glyercophosphocholine (GPC) and β nucleoside triphosphates (β-NTP). Resonances were corrected for their respective ^{31}P T_1 relaxation times (Table S2). One way analysis of variance (ANOVA) was used to assess the difference between the 3 groups with Tukey-Kramer HSD post-hoc tests using statistical software package JMP (SAS Institute, NC, USA). All values are reported as mean ± standard error.

Results

^{1}H MRS demonstrates steady-state metabolite concentrations that reflect increased glycolysis and truncated tricarboxylic acid (TCA) cycle in metastatic UOK262 cells

We first utilized ^{1}H MR spectroscopy (MRS) to interrogate the steady-state metabolite concentrations in HK2, UMRC6 and UOK262 cells. HK2 cells are derived from human renal proximal tubule cells (doubling time = 72–96 hours) (29). UMRC6 cells (doubling time = 43 hours) originate from a localized human clear cell RCC (30). Lastly, UOK262 cells were isolated from a metastasis of hereditary leiomyomatosis renal cell carcinoma (HLRCC) (doubling time = 23 hours) (31). HLRCC is an aggressive RCC characterized by mutation of the TCA cycle enzyme fumarate hydratase (FH). UOK262 cells therefore have markedly reduced oxidative phosphorylation and are highly glycolytic (31). Figure 1a illustrates the biochemical scheme of glycolysis and TCA cycle. Figure 1b shows the major steady-state intracellular metabolite concentrations, as measured by ^{1}H MRS, in the 3 cell lines. We found that the steady-state lactate concentration was significantly higher in the UOK262 cells compared to the UMRC6 or HK2 cells (both $P<0.05$). The increased steady-state lactate in the UOK262 cells is consistent with the FH mutation, which sharply attenuates the mitochondrial TCA cycle and concomitantly drives glycolysis for energy production (31).

The alanine concentration was lower in the two RCC cell lines compared to the HK2 cells, likely due to increased flux of pyruvate to lactate. We also found significantly increased glutamate and decreased aspartate concentration in the UOK262 cells compared to the other 2 cell lines. Glutamate is reversibly formed from α-ketoglutarate, a TCA cycle intermediate

proximal to fumarate. Aspartate is formed reversibly from oxaloacetate, a TCA intermediate distal to fumarate. In the UOK262 cells, the increased steady state glutamate and reduced aspartate are consistent with truncation of TCA cycle metabolism beyond fumarate, due to the FH mutation. The concentration of glycerophosphocholine (GPC), an abundant renal osmolyte (34), was similar among the 3 cell lines. Interestingly, we found that phosphocholine (PC) was significantly higher in the UMRC6 cells than the UOK262 cells. While PC has been used as a biomarker of tumor proliferation and aggressiveness in other types of cancers (35, 36), the levels of PC did not correlate with aggressiveness in the RCC cell lines in our study. PC is converted from choline by the enzyme choline kinase α (CHKA) in the phosphatidylcholine synthesis (Kennedy) pathway. A recent study reported that CHKA forms a complex with epidermal growth factor receptor (EGFR) in a c-Src-dependent manner, and functions cooperatively with EGFR and c-Src in regulating pathways critical to cell proliferation (37). Such required functional interaction among the three enzymes for cancer cell proliferation may in part explain the lack of direct correlation between the PC levels and proliferation rates/aggressiveness of the two RCC cell lines in our study.

24-hour labeling of cells with [1-^{13}C] glucose or [3-^{13}C] pyruvate in 2D cell cultures demonstrates increased flux to lactate in the metastatic UOK262 cells

To further characterize glycolysis and lactate production in the RCC cells, we investigated the flux from labeled [1-^{13}C] glucose to lactate in 2D cell cultures following 24-hour incubation. Figure 2a shows the scheme of ^{13}C labeled carbon atom transitions used to detect glucose metabolism to lactate. Glucose, the primary fuel for energy in cells, is taken up primarily *via* the glucose transporter 1 (GLUT1), and is converted to pyruvate and then lactate during glycolysis. Lactate is preferentially exported out of the cells via the monocarboxylate transporter 4 (MCT4) (38). Figure 2b and 2c demonstrate representative MR spectra of metabolites in the culture medium and intracellular compartment, respectively, of UOK262 cells following 24 hour labeling with [1-^{13}C] glucose. Figure 2d and 2e show the concentrations of ^{13}C labeled lactate in the medium and the intracellular compartment, respectively, of the 3 cell lines following incubation with [1-^{13}C] glucose. After 24 hour of incubation with [1-^{13}C] glucose, 99% of lactate was found in the extracellular medium. The concentration of ^{13}C lactate in the medium increased progressively from HK2 to UMRC6 to UOK262 cells, with the lactate concentration being nearly three-fold higher in the medium of UOK262 cells compared to that of the HK2 cells. The fractional enrichment (FE) of lactate was defined as the ^{13}C labeled lactate/(^{13}C labeled lactate + unlabeled lactate). The FE of lactate in the medium was 76 ± 1%, 65 ± 2% and 84 ± 1% in the HK2, UMRC6 and UOK262 cells, respectively. This implies that the predominant source of lactate in these cells is glucose, although there is a contribution from other carbon sources as well. The intracellular concentration of ^{13}C lactate was also significantly higher in the UOK262 cells compared to the UMRC6 or the HK2 cells ($p<0.05$). The intracellular FE of lactate was 62.5 ± 3.1%, 61.8 ± 1.5% and 78.6 ± 0.4% in the HK2, UMRC6 and UOK262 cells, respectively. The differential lactate FE in the intracellular compartment and the medium might be related to lactate compartmentalization in the cells. Such compartmentalization has been reported to exist in the brain and myocardium (39, 40). It is possible that one compartment of intracellular lactate originates predominantly from ^{13}C labeled glucose, and the subsequently labeled lactate is preferentially exported into the medium. Another compartment of lactate may derive from other sources such as from glutamine via glutaminolysis (41), and this compartment of lactate may not be as readily exported into the medium as that from glucose. The presence of lactate compartmentalization may also in part explain the higher FE of intracellular lactate in the UOK262 cells compared to the other cells. Because UOK262 have FH mutation with reduced TCA cycle metabolism, they are more likely to produce lactate from glycolysis than

from other pathways such as glutaminolysis that contains parts of the TCA cycle. This may explain the higher FE of the intracellular lactate from labeled glucose in the UOK262 cells. Taken together, the above findings confirmed that UOK262 cells are highly glycolytic with increased production of lactate. Interestingly, the ^{13}C lactate concentration was lower in the UMRC6 RCC cells relative to both HK2 and UOK262 cells. This was in agreement with the steady state intracellular lactate concentration data, which also showed a decreased lactate pool in UMRC6 cells compared to the other two cell lines (Figure 1b).

Hyperpolarized ^{13}C MRS demonstrates higher real-time pyruvate-to-lactate flux in RCC cells compared to normal HK2 cells, but lower pyruvate-to-lactate flux in the metastatic UOK262 cells than the localized UMRC6 cells

Given the dynamic nature of cellular metabolism, we then investigated the real-time pyruvate metabolism in the 3 cell lines utilizing HP ^{13}C MR. We performed our HP ^{13}C MR experiments using a bioreactor, a continuously perfused 3D cell culture system that provides a controlled and physiological setting for the cells. This system has been shown to produce highly reproducible HP MR data (28), and facilitates the characterization of hyperpolarized substrate to metabolite conversion. ^{31}P MR spectroscopy was employed to monitor changes in cell bioenergetics during the bioreactor studies. Representative ^{31}P spectra of the cells are shown in supplementary data (Figure S1). NMR signals for the nucleoside triphosphates (NTPs: γNTP, αNTP, and βNTP), phosphocholine (PC), inorganic phosphate (P_i), and glycerol phosphocholine (GPC) were readily visible. The total NTP content was unchanged following the injection of HP ^{13}C-pyruvate, indicating maintenance of cell viability during the course of the HP experiments. Figure 3 shows the PC/GPC ratios and PC+GPC concentration in the 3 cell lines. We found significantly higher PC+GPC concentration in the UMRC6 cells compared to the UOK262 cells ($p<0.05$), which was in agreement with the steady state ^{1}H data from 2D cell culture. In addition to monitoring cell energetics, ^{31}P spectroscopy also enables quantitative HP data analysis by normalizing the HP MR data with respect to the number of viable cells, through concomitant measurements of βNTP concentration *via* ^{31}P MRS.

Figure 4a illustrates the scheme of ^{13}C labeled carbon atom transitions used to detect ^{13}C-pyruvate metabolism during the HP MR experiment. After the injection of HP ^{13}C-pyruvate into the bioreactor, the real time pyruvate-to-lactate flux was assessed for all three cells lines. The data were fit to a two-state model of interconversion of pyruvate to lactate and the metabolic fluxes were calculated (28). Figure 4b shows fitted pyruvate-to-lactate flux and representative spectra of ^{13}C-pyruvate and lactate. The average fluxes, at a flow rate of 2.5ml/min in the bioreactor, for each of these cell lines are demonstrated in Figure 4c. The observed flux rate was significantly higher in the two RCC cell lines (UMRC6 and UOK262) as compared to the renal tubule cell line HK2 (UMRC6 vs. HK2 $p<0.0001$, UOK262 vs. HK2 $p=0.003$). Unexpectedly, the observed real time HP pyruvate-to-lactate flux for UOK262 cells (representative of metastatic RCC) was lower than that of the UMRC6 cells (representative of localized RCC). Similar to the flux data, the area under of the curve for the ^{13}C lactate was higher in the RCC cells than the normal renal tubule cells, but was lower in the UOK262 RCC cells than the UMRC6 RCC cells (supplemental data Table S1). Additional analysis of hyperpolarized ^{13}C dynamics of the cells perfused in the bioreactors was summarized in Table S1.

mRNA expression analysis demonstrates increased monocarboxylate transporter 4 (MCT4) in the metastatic UOK262 cells

To better understand the cellular processes underlying the HP pyruvate flux results, we then assayed the mRNA expression and enzyme activity level of LDHA, and the mRNA expression of MCT1 and MCT4 in the 3 cell lines. LDHA encodes the predominantly M

isoform of LDH, which catalyzes the conversion between pyruvate and lactate. MCT1 mediates the pyruvate transport into the cells, and MCT4 mediates the efflux of the lactate out of the cells (42). We found that the mRNA expression of LDHA was significantly higher in the UOK262 cells than the other two cell lines (Figure 5). For the LDH activity, K_m of the two RCC cell lines was significantly higher than that of the HK2 cells ($p<0.03$), but not significantly different between the UMRC6 and UOK262 RCC cells. The Vmax of UOK262 cells was significantly higher than that of HK2 cells ($p<0.05$). The mRNA expression of MCT1 was significantly higher in the UMRC6 cells (UMRC6 vs. HK2, p=0.0004; UMRC6 vs. UOK262, p=0.0002) while the MCT4 expression was significantly elevated in the UOK262 cells (UOK262 vs. HK2, p=0.001; UOK262 vs. UMRC6, p=0.02).

The higher HP pyruvate-to-lactate flux in UMRC6 cells, as compared to UOK262, was likely due, in part, to the higher MCT1 expression rather than the lactate pool size in the UMRC6 cells, as both the steady-state and 24 hour labeling data showed lower lactate pool size in the UMRC6 cells (Figure 1b and Figure 2e). Importantly, the differential expression of MCT4 may explain the apparent discrepancy between the real time HP pyruvate-to-lactate flux and the 24-hours labeling of lactate in the UOK262 cells compared to the UMRC6 cells. The UOK262 cells have an almost two-fold higher MCT4 expression compared to the UMRC6 cells, suggesting that they likely have more rapid MCT4-mediated export of lactate out of the cells. Rapid lactate efflux is essential for maintaining a neutral intracellular pH, and a high rate of glycolysis and lactate production over time. In contrast, UMRC6 cells have lower MCT4 expression, and likely slower rate of lactate export. Although UMRC6 cells have higher MCT1, these cells would be less able to maintain a high rate of lactate production over time due to buildup of intracellular lactate. Therefore, while the real time flux of pyruvate to lactate during the timeframe of the HP experiment was lower in the UOK262 cells than the UMRC6 cells, the higher MCT4 expression in the UOK262 cells likely resulted in more rapid lactate efflux and accounted for the significantly higher ^{13}C labeled lactate accumulated in the medium in the 24-hour labeling experiment. Over time, the large amount of labeled lactate accumulated in the medium of UOK262 cells likely diffused back into the cells down a gradient, and may explain the higher intracellular labeled lactate in the UOK262 cells compared to the UMRC6 cells. We postulate that, while such diffusion of lactate back into the cells may reduce further generation of labeled lactate, this process occurs after a large amount of lactate has already accumulated in the medium of the UOK262 cells. This accumulation of medium lactate and diffusion back into the UOK262 cells were likely accentuated in the 2D cell cultures where the extracellular lactate was not removed, in contrast to the bioreactor where the medium was continuously exchanged.

It is also important to note that while MCT1 may affect the HP lactate signal (both the intracellular and extracellular HP lactate) if it were the rate-limiting step in the pyruvate-to-lactate flux, the relative proportion of the intracellular versus extracellular HP lactate would be determined by MCT4, which modulates the lactate efflux. Additionally, lactate efflux in general is not expected to be significantly affected by MCT1, since most of the lactate produced in the cells is derived from glucose (transported via GLUT1) rather than pyruvate (transported via MCT1) uptake into the cells.

Hyperpolarized ^{13}C-pyruvate MR combined with flow rate modulation in the bioreactor demonstrate rapid efflux of lactate in the metastatic UOK262 cells

We then performed a second set of HP MR experiments using different flow rates in the bioreactor in order to investigate the real-time lactate efflux rate in the two RCC cell lines. At high flow rates, the extracellular lactate will more likely flow out of the NMR coil's sensitive volume and will not contribute to the MR signal, thereby decreasing the observed pyruvate-to-lactate flux (Figure 6a). It follows that the relative amount of extracellular

lactate (lactate in the medium) of the two RCC cell lines, which reflects the lactate efflux rate, can be inferred from the observed HP pyruvate-to-lactate flux at different flow rates. Figure 6b shows the pyruvate-to-lactate flux at different flow rates for the two RCC cells. For the UMRC6 cells, the mean observed HP pyruvate-to-lactate flux was 0.92 nmol/s per 10^6 cells at 1.3 ml/min, 0.90 nmol/s per 10^6 cells at 2.5ml/min, and 0.94 nmol/s per 10^6 cells at 3.8ml/min, all of which were not statistically different from one another. For the UOK262 cells, the mean observed HP pyruvate-to-lactate flux was 0.56 nmol/s per 10^6 cells at 1.3 ml/min, 0.51 nmol/s per 10^6 cells at 2.5ml/min, and 0.41 nmol/s per 10^6 cells at 3.8ml/min. These observed HP pyruvate-to-lactate flux for the UOK262 cells progressively decreased at higher flow rate, with a significant 20% decrease in the flux between the 2.5ml/min and 3.8ml/min flow rate ($p=0.01$). At the high flow rate of 3.8ml/min, the decreased pyruvate-to-lactate flux in the UOK262 cells indicated that these cells had more rapid lactate efflux and higher amount of extracellular lactate, which was readily removed from the NMR-sensitive region at high flow rate. The high flow rate should not have significantly limited the MCT1-mediated pyruvate uptake into the cells. This is because the injected HP pyruvate substrate available to the cells was expected to be in excess compared to MCT1, even at the high flow rate of 3.8ml/min. Indeed, the UMRC6 cells, with two-fold higher expression of MCT1 compared to the UOK262 cells, showed similar HP pyruvate-to-lactate flux at all 3 flow rates, indicating that the flow rates did not limit pyruvate uptake. The flow rate should also not have affected the enzymatic conversion of pyruvate to lactate in the cells. Taken together, the HP flux data at different flow rates strongly support the notion that the UOK262 cells have increased MCT4-mediated lactate efflux out of the cells.

Additionally, we incubated the UMRC6 and UOK262 cells for 2 hours in medium containing [3-^{13}C] pyruvate, and observed 0.47 ± 0.05 versus 2.32 ± 0.27 μmols/10^6 cells of ^{13}C labeled lactate in the medium of UMRC6 versus UOK262 cells. This > 5-fold increase in the extracellular lactate of the UOK262 cells further verifies that lactate derived from labeled pyruvate is produced and transported out of the cells at a higher rate in the UOK262 cells compared to the UMRC6 cells.

Discussion

There is increasing evidence that RCCs are among those tumors strongly linked to abnormal metabolism, a feature that may be exploited therapeutically. In this work, we investigated the pyruvate metabolism in perfused human RCC cells using a clinically translatable HP ^{13}C MR probe, and interrogated both the biochemical basis of the observed HP MR data and its relationship to cancer aggressiveness. We found higher pyruvate-to-lactate flux, consistent with increased glycolysis, in RCC cells compared to normal renal proximal tubule cells. We further noted that a key feature distinguishing the localized UMRC6 from the metastatic UOK262 RCC cells is the lactate efflux rate, and that, importantly, this feature can be noninvasively depicted via real-time monitoring of HP ^{13}C-pyruvate-to-lactate flux.

Lactate efflux is predominantly mediated by MCT4, which is a proton-coupled lactate transporter (42), exporting lactate and H+ in the same direction out of the cells. Rapid lactate efflux serves to maintain high levels of glycolysis in cancer cells, and concurrently acidifies the extracellular environment (11). Low extracellular pH supports invasion and metastasis, perhaps due to pH-dependent activation of cathepsins and metalloproteinases that degrade extracellular matrix and basement membranes (43). In this study, we found that the metastatic UOK262 cells have significantly higher MCT4 expression compared to the localized UMRC6 cells, and also have more rapid export of lactate out of the cells. UOK262 cells have mutations in the TCA enzyme FH, which leads to an uncommon and highly aggressive hereditary RCC. However, recent studies have shown that FH mRNA and protein expression are reduced in clear cell RCC, the most common histological variant of kidney

cancer, promoting tumor migration and invasion (44). The reduced FH leads to accumulation of hypoxia inducible factor-2 alpha (HIF-2α) (45), a transcription factor known to promote renal carcinogenesis in part by up-regulating glycolysis (17). Thus, the metabolic changes observed in the UOK262 cells are likely not unique to this particular RCC type, and the MCT4-mediated lactate efflux may be an important determinant of RCC aggressiveness in general. Supporting this hypothesis, a recent study showed that MCT4 protein expression in primary clear cell RCCs was associated with poorer relapse-free survival, and correlated with Fuhrman nuclear grade (46). Additionally, MCT4 knockdown RCC cell lines had reduced intracellular pH, impaired proliferation and increased apoptosis (46). These studies indicate that MCT4 targeting may also be an important strategy for the treatment of RCCs.

We showed that the MCT4-mediated lactate efflux in living cells can be explored noninvasively using HP ^{13}C MR. This was accomplished by monitoring the real time cellular pyruvate-to-lactate fluxes under different flow rates in the bioreactor. While our study utilized an *ex vivo* system, interrogation of lactate export using HP ^{13}C MR can be achieved *in vivo*. For example, it is possible to measure the tumoral extracellular or interstitial pH, which in part reflects the amount of exported lactate, using HP ^{13}C bicarbonate MR (47, 48). Moreover, it is possible to discriminate the local environment of HP metabolites using diffusion weighting *in vivo* (49, 50). Future studies will develop diffusion-weighted HP MR that can directly quantify the relative amount of intracellular versus extracellular lactate.

While total lactate levels can also be monitored using ^{1}H MRS, this approach has limited utility in the metabolic evaluation of renal tumors, particularly in the *in vivo* setting. Lactate and lipid peaks usually overlap such that the assessment of lactate is challenging even when methods for lipid suppression are applied. More importantly, the real time metabolic fluxes, influenced by enzymatic and transporter expression, cannot be captured using ^{1}H MRS.

In conclusion, we have demonstrated that HP ^{13}C-pyruvate MRS enables real-time observation of differential lactate efflux, mediated by MCT4, in living RCC cells of varying aggressiveness. Importantly, as MCT4 and lactate efflux are implicated in the pathogenesis of many types of cancers, HP ^{13}C MRS has the potential to noninvasively interrogate tumor aggressiveness and treatment efficacy in a broad range of cancers.

Supplementary Material

Refer to Web version on PubMed Central for supplementary material.

Acknowledgments

Grant Support: This work was supported by NIH P41EB013598 (to JK), R01CA166766 (to DMW), K99EB014328 (to KRK), Department of Defense Peer Reviewed Cancer Research Concept Award (to ZJW), Radiological Society of North America Scholar grant (to ZJW).

References

1. Patard JJ. Incidental renal tumours. Curr Opin Urol. 2009; 19(5):454–8. [PubMed: 19571758]
2. Volpe A, Mattar K, Finelli A, Kachura JR, Evans AJ, Geddie WR, et al. Contemporary results of percutaneous biopsy of 100 small renal masses: a single center experience. J Urol. 2008; 180(6): 2333–7. [PubMed: 18930274]
3. Shannon BA, Cohen RJ, de Bruto H, Davies RJ. The value of preoperative needle core biopsy for diagnosing benign lesions among small, incidentally detected renal masses. J Urol. 2008; 180(4): 1257–61. discussion 61. [PubMed: 18707712]

4. Eggener SE, Yossepowitch O, Pettus JA, Snyder ME, Motzer RJ, Russo P. Renal cell carcinoma recurrence after nephrectomy for localized disease: predicting survival from time of recurrence. J Clin Oncol. 2006; 24(19):3101–6. [PubMed: 16809736]
5. Jewett MA, Mattar K, Basiuk J, Morash CG, Pautler SE, Siemens DR, et al. Active surveillance of small renal masses: progression patterns of early stage kidney cancer. Eur Urol. 2011; 60(1):39–44. [PubMed: 21477920]
6. Crispen PL, Viterbo R, Boorjian SA, Greenberg RE, Chen DY, Uzzo RG. Natural history, growth kinetics, and outcomes of untreated clinically localized renal tumors under active surveillance. Cancer. 2009; 115(13):2844–52. [PubMed: 19402168]
7. Lam JS, Shvarts O, Leppert JT, Figlin RA, Belldegrun AS. Renal cell carcinoma 2005: new frontiers in staging, prognostication and targeted molecular therapy. J Urol. 2005; 173(6):1853–62. [PubMed: 15879764]
8. Sun M, Shariat SF, Cheng C, Ficarra V, Murai M, Oudard S, et al. Prognostic factors and predictive models in renal cell carcinoma: a contemporary review. Eur Urol. 2011; 60(4):644–61. [PubMed: 21741163]
9. Millet I, Doyon FC, Hoa D, Thuret R, Merigeaud S, Serre I, et al. Characterization of small solid renal lesions: can benign and malignant tumors be differentiated with CT? AJR Am J Roentgenol. 2011; 197(4):887–96. [PubMed: 21940576]
10. Cooperberg MR, Mallin K, Ritchey J, Villalta JD, Carroll PR, Kane CJ. Decreasing size at diagnosis of stage 1 renal cell carcinoma: analysis from the National Cancer Data Base, 1993 to 2004. J Urol. 2008; 179(6):2131–5. [PubMed: 18423754]
11. Gatenby RA, Gillies RJ. Why do cancers have high aerobic glycolysis? Nat Rev Cancer. 2004; 4(11):891–9. [PubMed: 15516961]
12. Warburg O. On the origin of cancer cells. Science. 1956; 123(3191):309–14. [PubMed: 13298683]
13. Vander Heiden MG, Cantley LC, Thompson CB. Understanding the Warburg effect: the metabolic requirements of cell proliferation. Science. 2009; 324(5930):1029–33. [PubMed: 19460998]
14. Costello LC, Franklin RB. 'Why do tumour cells glycolyse?': from glycolysis through citrate to lipogenesis. Mol Cell Biochem. 2005; 280(1–2):1–8. [PubMed: 16511951]
15. Gatenby RA, Gawlinski ET, Gmitro AF, Kaylor B, Gillies RJ. Acid-mediated tumor invasion: a multidisciplinary study. Cancer Res. 2006; 66(10):5216–23. [PubMed: 16707446]
16. Unwin RD, Craven RA, Harnden P, Hanrahan S, Totty N, Knowles M, et al. Proteomic changes in renal cancer and co-ordinate demonstration of both the glycolytic and mitochondrial aspects of the Warburg effect. Proteomics. 2003; 3(8):1620–32. [PubMed: 12923786]
17. Semenza GL. HIF-1 mediates the Warburg effect in clear cell renal carcinoma. J Bioenerg Biomembr. 2007; 39(3):231–4. [PubMed: 17551816]
18. Langbein S, Frederiks WM, zur Hausen A, Popa J, Lehmann J, Weiss C, et al. Metastasis is promoted by a bioenergetic switch: new targets for progressive renal cell cancer. Int J Cancer. 2008; 122(11):2422–8. [PubMed: 18302154]
19. Gao H, Dong B, Liu X, Xuan H, Huang Y, Lin D. Metabonomic profiling of renal cell carcinoma: high-resolution proton nuclear magnetic resonance spectroscopy of human serum with multivariate data analysis. Anal Chim Acta. 2008; 624(2):269–77. [PubMed: 18706333]
20. Ardenkjaer-Larsen JH, Fridlund B, Gram A, Hansson G, Hansson L, Lerche MH, et al. Increase in signal-to-noise ratio of > 10,000 times in liquid-state NMR. Proc Natl Acad Sci U S A. 2003; 100(18):10158–63. [PubMed: 12930897]
21. Chen AP, Albers MJ, Cunningham CH, Kohler SJ, Yen YF, Hurd RE, et al. Hyperpolarized C-13 spectroscopic imaging of the TRAMP mouse at 3T-initial experience. Magn Reson Med. 2007; 58(6):1099–106. [PubMed: 17969006]
22. Cunningham CH, Chen AP, Albers MJ, Kurhanewicz J, Hurd RE, Yen YF, et al. Double spin-echo sequence for rapid spectroscopic imaging of hyperpolarized (13)C. J Magn Reson. 2007; 187(2): 357–62. [PubMed: 17562376]
23. Hu S, Lustig M, Chen AP, Crane J, Kerr A, Kelley DA, et al. Compressed sensing for resolution enhancement of hyperpolarized (13)C flyback 3D-MRSI. J Magn Reson. 2008
24. Kurhanewicz J, Bok R, Nelson SJ, Vigneron DB. Current and Potential Applications of Clinical 13C MR Spectroscopy. J Nucl Med. 2008; 49(3):341–4. [PubMed: 18322118]

25. Golman K, Petersson JS. Metabolic imaging and other applications of hyperpolarized 13C1. Acad Radiol. 2006; 13(8):932–42. [PubMed: 16843845]
26. Albers MJ, Bok R, Chen AP, Cunningham CH, Zierhut ML, Zhang VY, et al. Hyperpolarized 13C lactate, pyruvate, and alanine: noninvasive biomarkers for prostate cancer detection and grading. Cancer Res. 2008; 68(20):8607–15. [PubMed: 18922937]
27. Zierhut, M.; Chen, A.; Bok, R.; Albers, M.; Zhang, V.; Pels, P., et al. Kinetic Modeling of Hyperpolarized 13C1-Pyruvate Metabolism Using Dynamic Magnetic Resonance Spectroscopy. Proc of the Intn'l Soc of Mag Res in Med; Berlin, Germany. 2007.
28. Keshari KR, Kurhanewicz J, Jeffries RE, Wilson DM, Dewar BJ, Van Criekinge M, et al. Hyperpolarized (13)C spectroscopy and an NMR-compatible bioreactor system for the investigation of real-time cellular metabolism. Magn Reson Med. 2010; 63(2):322–9. [PubMed: 20099325]
29. Ryan MJ, Johnson G, Kirk J, Fuerstenberg SM, Zager RA, Torok-Storb B. HK-2: an immortalized proximal tubule epithelial cell line from normal adult human kidney. Kidney Int. 1994; 45(1):48–57. [PubMed: 8127021]
30. Grossman HB, Wedemeyer G, Ren LQ. Human renal carcinoma: characterization of five new cell lines. J Surg Oncol. 1985; 28(3):237–44. [PubMed: 4038766]
31. Yang Y, Valera VA, Padilla-Nash HM, Sourbier C, Vocke CD, Vira MA, et al. UOK 262 cell line, fumarate hydratase deficient (FH-/FH-) hereditary leiomyomatosis renal cell carcinoma: in vitro and in vivo model of an aberrant energy metabolic pathway in human cancer. Cancer Genet Cytogenet. 2010; 196(1):45–55. [PubMed: 19963135]
32. Beckonert O, Keun HC, Ebbels TM, Bundy J, Holmes E, Lindon JC, et al. Metabolic profiling, metabolomic and metabonomic procedures for NMR spectroscopy of urine, plasma, serum and tissue extracts. Nat Protoc. 2007; 2(11):2692–703. [PubMed: 18007604]
33. Chandrasekaran P, Seagle C, Rice L, Macdonald J, Gerber DA. Functional analysis of encapsulated hepatic progenitor cells. Tissue Eng. 2006; 12(7):2001–8. [PubMed: 16889528]
34. Nakanishi T, Burg MB. Osmoregulation of glycerophosphorylcholine content of mammalian renal cells. Am J Physiol. 1989; 257(4 Pt 1):C795–801. [PubMed: 2801928]
35. Shah T, Wildes F, Penet MF, Winnard PT Jr, Glunde K, Artemov D, et al. Choline kinase overexpression increases invasiveness and drug resistance of human breast cancer cells. NMR Biomed. 2010; 23(6):633–42. [PubMed: 20623626]
36. Eliyahu G, Kreizman T, Degani H. Phosphocholine as a biomarker of breast cancer: molecular and biochemical studies. Int J Cancer. 2007; 120(8):1721–30. [PubMed: 17236204]
37. Miyake T, Parsons SJ. Functional interactions between Choline kinase alpha, epidermal growth factor receptor and c-Src in breast cancer cell proliferation. Oncogene. 2012; 31(11):1431–41. [PubMed: 21822308]
38. Dimmer KS, Friedrich B, Lang F, Deitmer JW, Broer S. The low-affinity monocarboxylate transporter MCT4 is adapted to the export of lactate in highly glycolytic cells. Biochem J. 2000; 350(Pt 1):219–27. [PubMed: 10926847]
39. Sickmann HM, Schousboe A, Fosgerau K, Waagepetersen HS. Compartmentation of lactate originating from glycogen and glucose in cultured astrocytes. Neurochem Res. 2005; 30(10): 1295–304. [PubMed: 16341591]
40. Chatham JC, Forder JR. Metabolic compartmentation of lactate in the glucose-perfused rat heart. The American journal of physiology. 1996; 270(1 Pt 2):H224–9. [PubMed: 8769755]
41. Wise DR, Thompson CB. Glutamine addiction: a new therapeutic target in cancer. Trends Biochem Sci. 2010; 35(8):427–33. [PubMed: 20570523]
42. Kroemer G, Pouyssegur J. Tumor cell metabolism: cancer's Achilles' heel. Cancer Cell. 2008; 13(6):472–82. [PubMed: 18538731]
43. Swietach P, Vaughan-Jones RD, Harris AL. Regulation of tumor pH and the role of carbonic anhydrase 9. Cancer Metastasis Rev. 2007; 26(2):299–310. [PubMed: 17415526]
44. Sudarshan S, Shanmugasundaram K, Naylor SL, Lin S, Livi CB, O'Neill CF, et al. Reduced expression of fumarate hydratase in clear cell renal cancer mediates HIF-2alpha accumulation and promotes migration and invasion. PLoS One. 2011; 6(6):e21037. [PubMed: 21695080]

45. Pollard PJ, Briere JJ, Alam NA, Barwell J, Barclay E, Wortham NC, et al. Accumulation of Krebs cycle intermediates and over-expression of HIF1alpha in tumours which result from germline FH and SDH mutations. Hum Mol Genet. 2005; 14(15):2231–9. [PubMed: 15987702]

46. Gerlinger M, Santos CR, Spencer-Dene B, Martinez P, Endesfelder D, Burrell RA, et al. Genome-wide RNA interference analysis of renal carcinoma survival regulators identifies MCT4 as a Warburg effect metabolic target. J Pathol. 2012; 227(2):146–56. [PubMed: 22362593]

47. Gallagher FA, Kettunen MI, Day SE, Hu DE, Ardenkjaer-Larsen JH, Zandt R, et al. Magnetic resonance imaging of pH in vivo using hyperpolarized 13C-labelled bicarbonate. Nature. 2008; 453(7197):940–3. [PubMed: 18509335]

48. Wilson DM, Keshari KR, Larson PE, Chen AP, Hu S, Van Criekinge M, et al. Multi-compound polarization by DNP allows simultaneous assessment of multiple enzymatic activities in vivo. J Magn Reson. 2010; 205(1):141–7. [PubMed: 20478721]

49. Larson PE, Kerr AB, Reed GD, Hurd RE, Kurhanewicz J, Pauly JM, et al. Generating super stimulated-echoes in MRI and their application to hyperpolarized C-13 diffusion metabolic imaging. IEEE Trans Med Imaging. 2012; 31(2):265–75. [PubMed: 22027366]

50. Chen AP, Hurd RE, Cunningham CH. Spin tagging for hyperpolarized (1)(3)C metabolic studies. J Magn Reson. 2012; 214(1):319–23. [PubMed: 22050921]

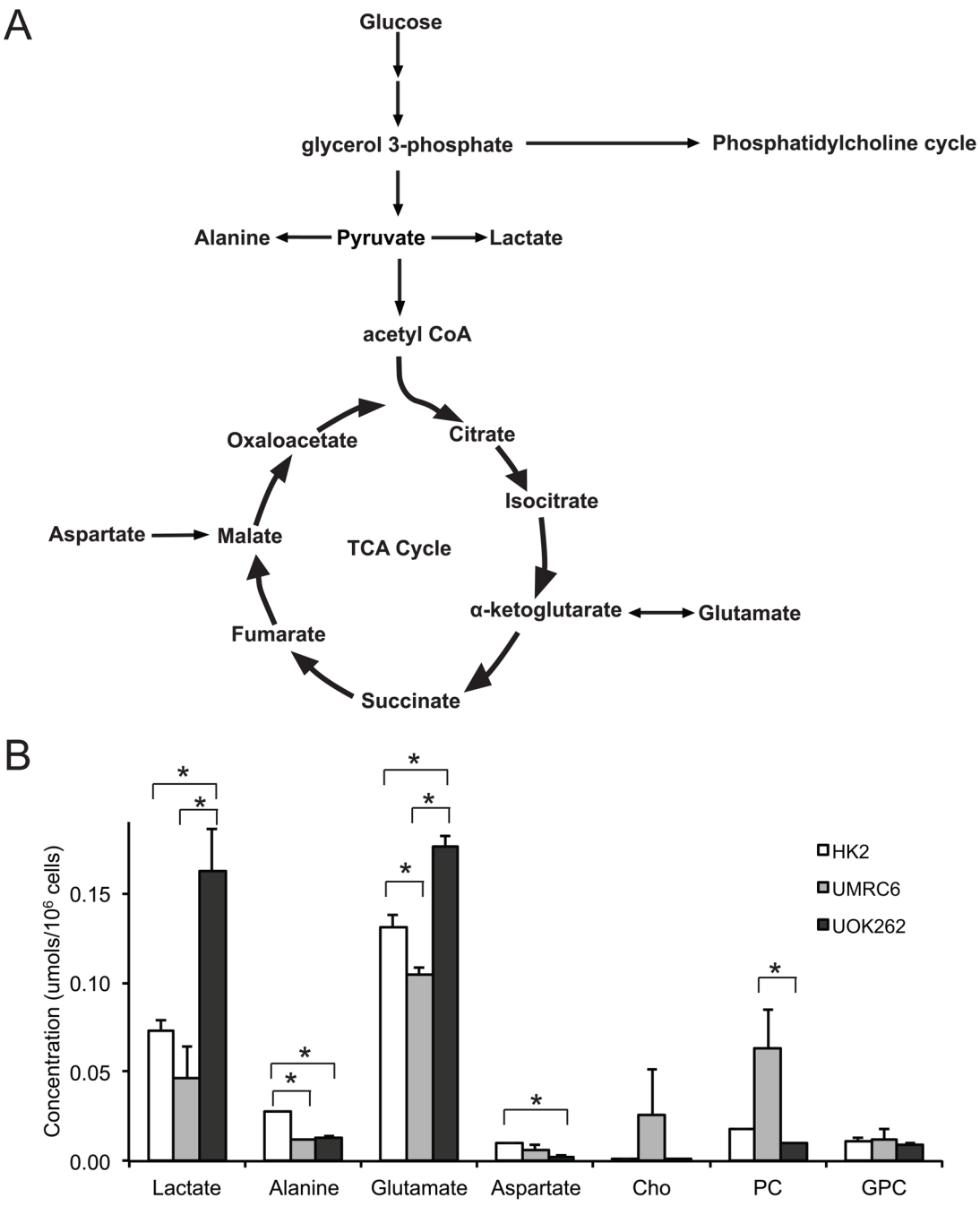

Figure 1.

Steady state major metabolites in the 3 cell lines. (A) Biochemical scheme of glycolysis and tricarboxylic acid (TCA) cycle. (B) Steady state concentrations of major metabolites, as measured by ^{1}H MRS, in the 3 cell lines (N=5 each). All values are reported as mean ± std. err. * denotes significant difference ($p<0.05$).

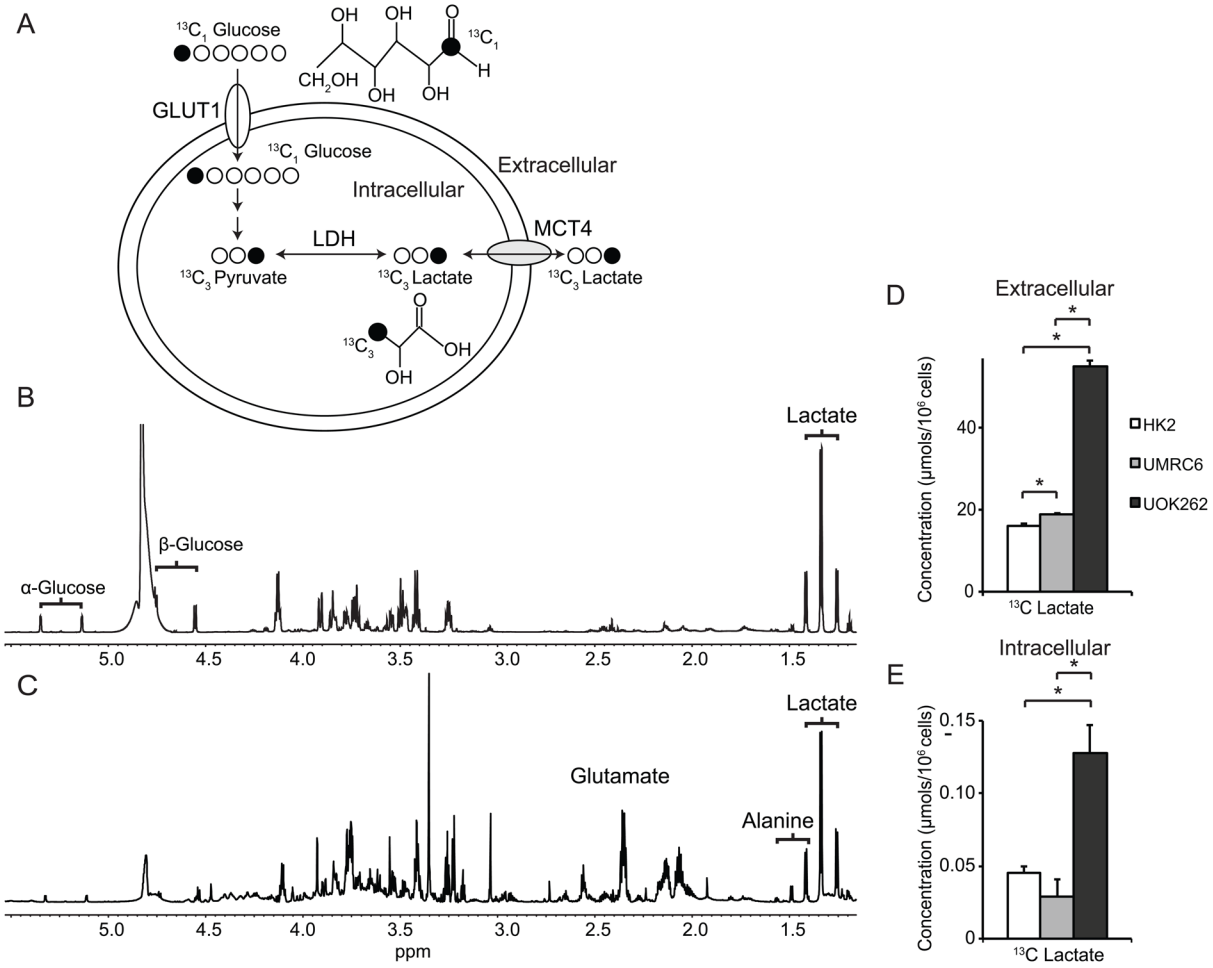

Figure 2.

^{13}C labeled lactate in the media and intracellular compartment of the 3 cell lines following 24 hour incubation with [1-^{13}C] glucose. (A) Biochemical scheme illustrating ^{13}C labeled carbon atom transitions used to detect glucose metabolism to lactate. Representative ^{1}H MR spectra of metabolites in the medium (B) and intracellular compartments (C) of UOK262 following 24 hour labeling with [1-^{13}C] glucose. The brackets indicate the ^{13}C satellites of each metabolite. Concentrations of ^{13}C labeled lactate in the media (D) and intracellular compartment (E) of the 3 cell lines following incubation with [1-^{13}C] glucose (N=5 each). All values are reported as mean ± std. err. * denotes significant difference ($p<0.05$).

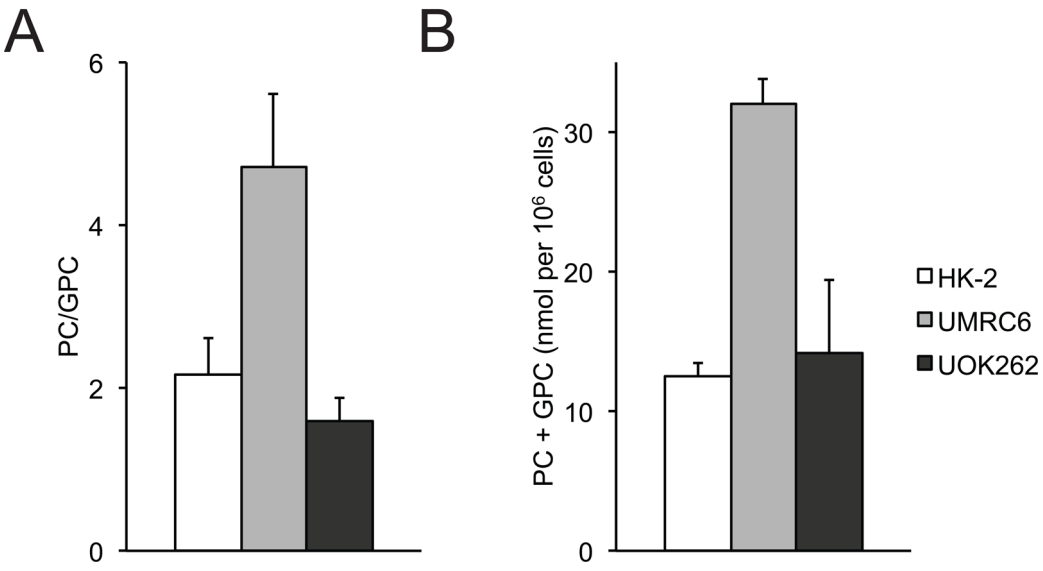

Figure 3.

Phosphocholine metabolites in the 3 cell lines. PC/GPC ratios (A), and PC+GPC concentration (B) of cells encapsulated and perfused in a bioreactor (N=5 each). All values are reported as mean ± std. err. PC – phosphocholine, GPC – glycerophosphocholine.

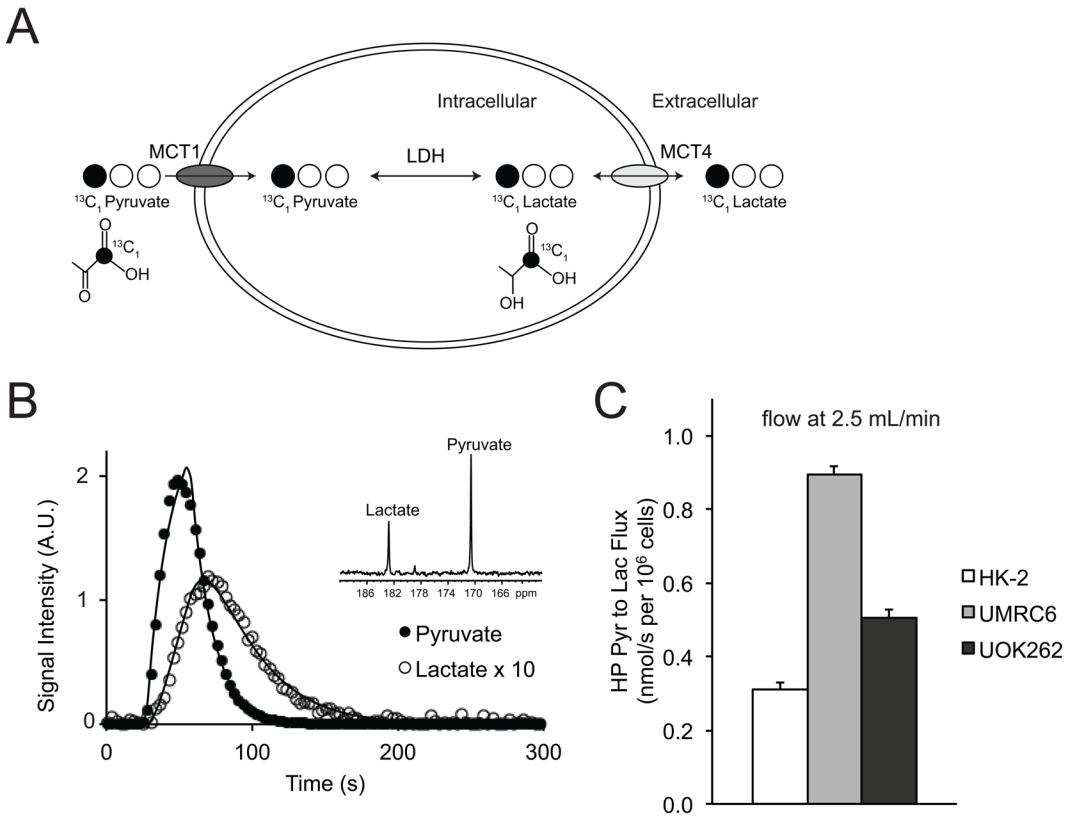

Figure 4.

Dynamic HP pyruvate-to-lactate flux in the 3 cell lines. (A) Scheme of ^{13}C labeled carbon atom transitions used to detect C_1 labeled pyruvate metabolism during the hyperpolarized experiment. (B) Fitted pyruvate-to-lactate flux and representative spectra (inset) of ^{13}C-pyruvate and lactate in the UMRC6 cells. (C) Comparison of observed real time HP pyruvate-to-lactate flux in the 3 cell lines at a flow rate of 2.5ml/min in the bioreactor (N=5 each). All values are reported as mean ± std. err.

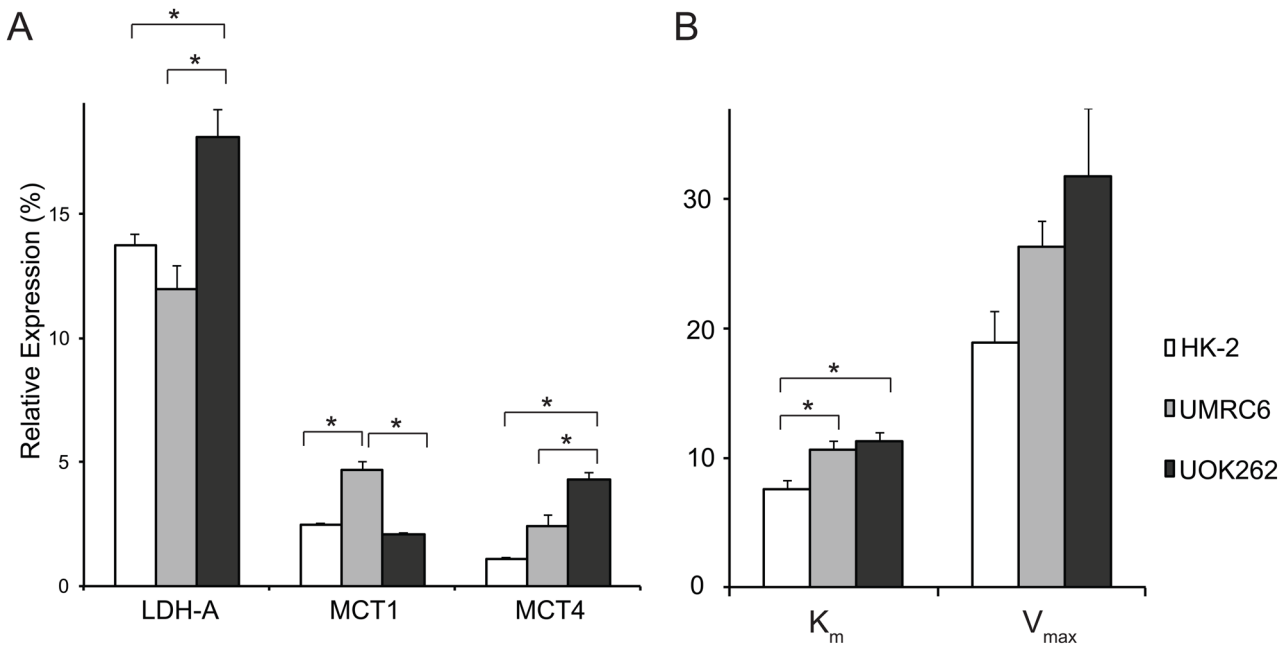

Figure 5.

Analysis of relevant enzyme expression/activity and transporter expression in the 3 cell lines. (A) mRNA expression of lactate dehydrogenase A (LDHA) and monocarboxylate transporters 1 and 4 (MCT1 and MCT4), relative to internal beta-actin expression, in the 3 cell lines (N=6 each). (B) LDH activity as measured by Km (μmols Pyruvate/10^6 cells) and V_{max} (μmols NADH/sec/10^6 cells) in the 3 cell lines (N= 6 each). All values are reported as mean ± std. err. * denotes significant difference ($p<0.05$).

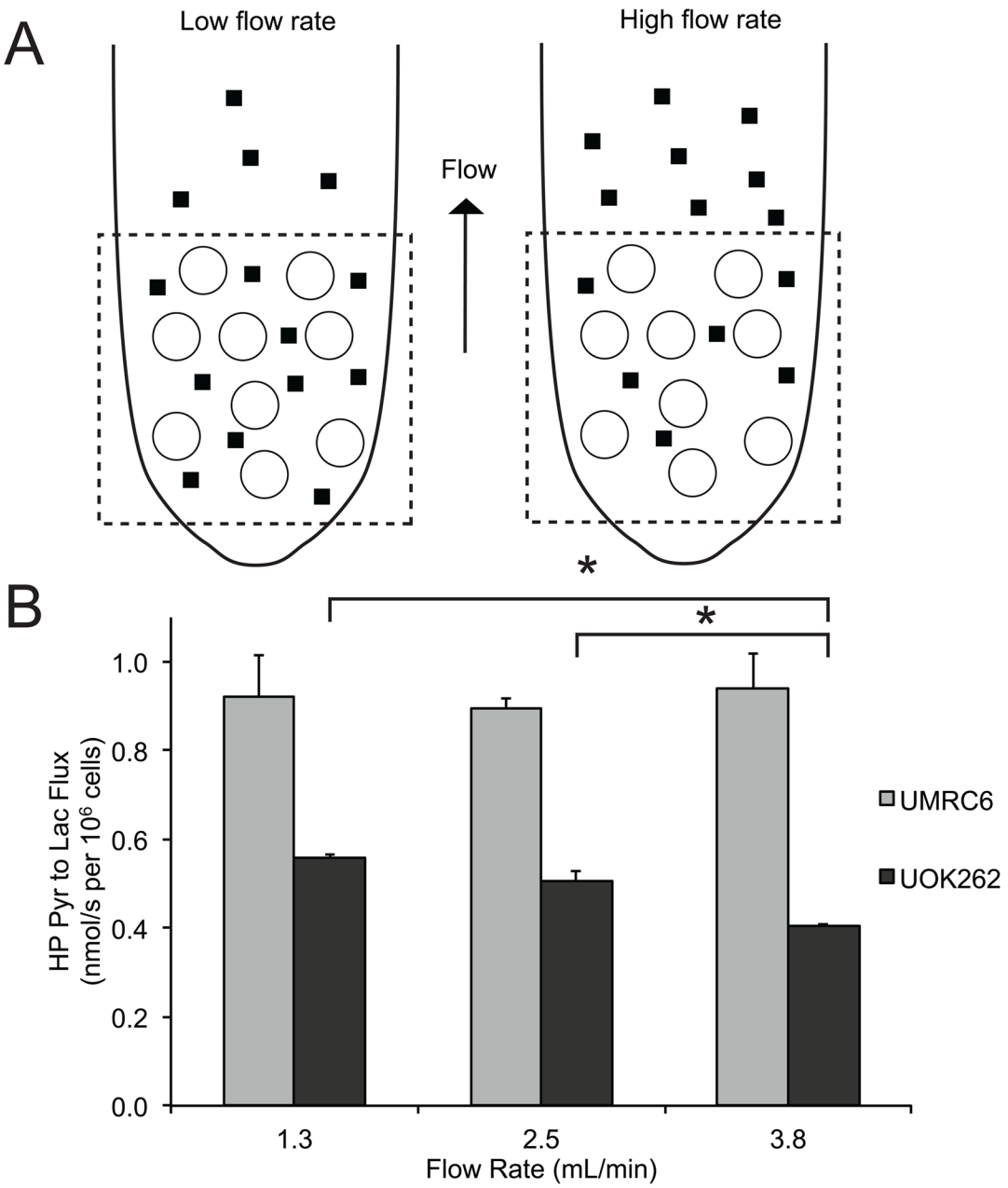

Figure 6.

Dynamic HP pyruvate-to-lactate flux in the RCC cells following flow rate modulation in the bioreactor. (A) Schematic illustrating the relationship between flow rates and observed HP pyruvate-to-lactate flux in the bioreactor. At high flow rates, the extracellular lactate will more likely to flow out of the NMR coil's sensitive volume and will not contribute to the MR signal, thereby decreasing the observed pyruvate-to-lactate flux. The dotted square represents NMR sensitive region. ○ denotes encapsulated microspheres containing cells. ▮ denotes extracellular lactate. (B) HP pyruvate-to-lactate flux of UOK262 and UMRC6 cells at 3 different flow rate (N=5 each). There is a decreasing trend in observed pyruvate-to-lactate flux with increasing flow rate for UOK262 cells. All values are reported as mean ± std. err. * denotes significance ($p<0.05$).